

Soot Formation from Laminar Ethylene/Air Diffusion Flames at Pressures from 1 to 8 atm

Hongsheng Guo^a, Zhongzhu Gu^b, Kevin A. Thomson^a, Gregory J. Smallwood^a

^aNational Research Council of Canada, Ottawa, Ontario K1A 0R6, Canada

^bNanjing Normal University, Nanjing 210042, Jiangsu, P.R. China

1 Introduction

Soot is one of primary pollutants emitted during the combustion of hydrocarbon fuels. Since most practical combustion devices operate at higher pressure conditions, it is of great importance to understand the effect of pressure on soot formation.

Flower and Bowman [1] investigated soot formation in ethylene/air axisymmetric laminar diffusion flames at pressures from 1 to 10 atm by measuring the attenuation of laser light across the flame diameter. They observed that the maximum line-of-sight integrated soot volume fraction was proportional to the pressure raised to an exponent of about 1.2. McCrain and Roberts [2] measured soot formation in laminar ethylene and methane diffusion flames and found that dependence of peak soot volume fraction on pressure was different from that of line-of-sight integrated soot volume fraction for both fuels. Recently, Gülder and collaborators [3-6] experimentally investigated soot formation in laminar diffusion flames at high pressures for various fuels. They also found that the peak carbon conversion, the percentage of fuel's carbon content converted to soot, was proportional to pressure to an n th power, with n slightly differing for different fuels and at different pressure range.

Relatively, only a few numerical studies on the effect of pressure on soot formation have been conducted. Zhang and Ezekoye [7] numerically investigated soot formation at elevated pressures in a methane/air diffusion flame using reduced gas phase chemistry and showed that increased density resulted in the higher soot concentration. Liu et al. [8] and Charest et al. [9] numerically investigated soot formation in methane/air and ethylene/air diffusion flames, respectively, by using relatively detailed gas phase chemistry. They also concluded that the effect of pressure on soot formation was largely attributed to the increase in mixture density. All these numerical studies [7-9] used simplified two-equation soot model and assumed that soot inception and surface growth solely depended on local concentration of acetylene (C_2H_2). It has been previously shown that acetylene based soot models failed to capture some experimentally observed important phenomena due to the neglect of some key steps in soot inception and surface growth [10,11]. Therefore, it is of great interest to further numerically investigate the effect of pressure on soot formation using a more detailed soot model.

In this paper, soot formation in laminar ethylene/air diffusion flames is investigated by experiment and numerical simulation using complex gas phase chemistry and a relatively detailed soot model. The paper starts with the description of experimental methodology, followed by the numerical model. Then the experimental and numerical results are demonstrated and compared, and discussion on the

mechanism of the effect of pressure on soot formation is provided by analyzing the details of the numerical data.

2 Experimental Methodology

The flames were experimentally generated by a coflow laminar diffusion flame burner that is installed inside a pressure vessel. The burner consists of a fuel nozzle with inner diameter of 2.29 mm and outer diameter of 4.76 mm and an annular concentric air tube with inner diameter of 25.4 mm. A tapered fuel nozzle exit was designed to reduce recirculation from the burner tip, which results in an exit diameter of 3.06 mm for the fuel nozzle. Sintered metal foam elements are included in the fuel and air nozzles to straighten and reduce instabilities in the flow. The pressure vessel is a large cylinder, with an internal height of 600 mm and an internal diameter of 240 mm. It was designed for working pressures up to 100 atm. Physical access to the vessel is possible through the upper and lower flanges. Optical access to the vessel is possible through three viewing ports so that line-of-sight measurements are possible. Further details of the burner and pressure vessel can be found elsewhere [3].

Soot volume fraction was measured using the diffuse-light two-dimensional line-of-sight attenuation (LOSA) optical diagnostic method [12]. The light source for the experiments is a mercury arc lamp diffused by an integrating sphere and imaged to the flame center with a pair of achromatic lens doublets. The flame center was imaged with a commercial 150 mm focal length cameralens (Sigma Corporation) onto a CCD array filtered with a 450 nm narrow band filter. The magnification of the system is such that each square pixel images a square of $33 \times 33 \mu\text{m}^2$. The data is binned horizontally and vertically to reduce shot noise and the final spatial resolution is $132 \times 528 \mu\text{m}^2$. A soot refractive index light absorption function, $E(m)$, of 0.27 was used in the data analysis.

The measurement was conducted at pressures of 1, 3, 6 and 8 atm for ethylene/air diffusion flames. Higher pressures would result in smoking flames and thus were not conducted. The mass flow rates of ethylene and air were kept constant at 0.48 mg/s and 0.40 g/s, respectively.

3 Numerical Scheme and Soot Model

The flames were modeled by numerical simulation. The low Mach number assumption was adopted. The SIMPLE numerical scheme [13] was used. The diffusion terms in the conservation equations were discretized by the central difference method and the convective terms were discretized by the power law method [13]. The discretized governing equations of gas species and soot moments were, respectively, solved in a fully coupled fashion at each control volume. Those of momentum, energy and pressure correction were solved using the tri-diagonal matrix algorithm.

Due to radial symmetry, only half of the flame was simulated. The computational domain covers an area from 0 to 12 mm in the radial (r) direction and 0 to 28 mm in the axial (z) direction. The inflow boundary ($z = 0$ mm) corresponds to the region immediately above the fuel nozzle. In total, 160 (z) \times 218 (r) non-uniform grids were used in the simulations, with finer grids ($0.03 \times 0.03 \text{ mm}^2$) being placed in the primary reaction zone and near the fuel nozzle exit region. The symmetric condition was used for the centerline in the simulation. The free slip boundary condition was used for the side boundary, and zero-gradient condition was employed for the top outlet. At the bottom of the domain, uniform velocities, temperatures and compositions were specified for the center fuel tube region and outer concentric space, respectively, based on supplied fuel and air. Radiation heat transfer was calculated by the discrete ordinate method coupled to a statistical narrow-band correlated-K (SNBCK) based wide band model for the radiating properties of CO, CO₂, H₂O and soot [14]. Other details of the numerical methods can be found from our previous publications [10,11].

The formation and evolution of soot particles were simulated by the method of moments [15]. Six concentration moments were used. The inception of soot particles is assumed to be due to the coalescence of two large size PAH molecules, pyrene (A4). Then the particle size increases or decreases due to the particle coagulation, surface growth and oxidation. The gas phase chemistry and the calculation methods for the particle inception, coagulation, surface growth and oxidation are

basically those developed by Appel et al. [16]. However, some modifications have been made for gas phase chemistry and surface growth calculation because the original method and chemistry significantly underpredicted soot volume fraction. More details of the soot model and the modifications to the base gas-phase chemistry can be found elsewhere [11].

4 Results and Discussion

Figure 1 displays the measured and calculated radial distributions of soot volume fraction (SVF) at four axial heights that cover the primary soot formation region for studied flames. It is observed that the results from simulation and experiment are qualitatively consistent. For all pressures, with the increase in axial height, soot volume fraction first increases and then decreases. The maximum soot volume fractions appear in an annular wing region for most flames, except for the flame at pressure of 1 atm (note that soot volume fraction at 1 atm is so small that it cannot be clearly observed from Fig. 1). Both experiment and simulation show that at each axial height, with the increase in pressure, soot volume fraction quickly increases and the radial position of the maximum soot volume fraction moves toward the centerline. These are qualitatively consistent with the results from previous experimental and numerical studies [8,9] for other high pressure flames.

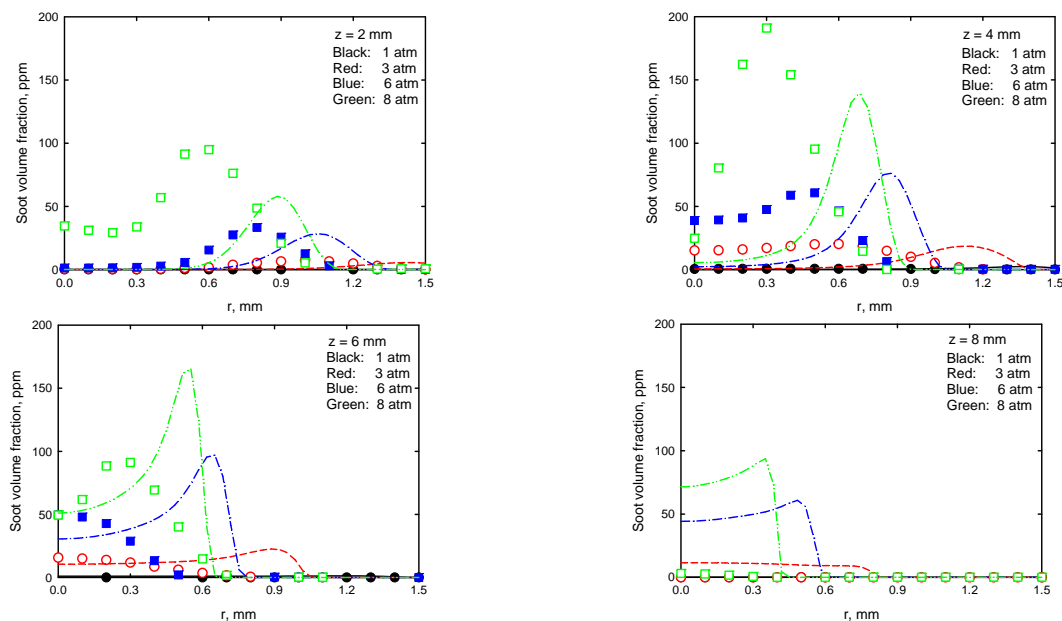


Fig. 1 Measured (symbols) and calculated (lines) soot volume fractions at different axial heights.

Quantitative differences exist between experiment and simulation. The calculated radial position of the maximum soot volume fraction at each axial height is farther from centerline than the measured. At $z = 8$ mm, almost no soot can be observed by experiment, but simulation results still shows significant soot at all pressures, suggesting that simulation predicted higher visible flame heights than measured. Figure 2 shows the variations of the peak soot volume fraction, the peak area-integrated soot volume fraction ($2\pi \int f_v r dr$, with f_v being local soot volume fraction) and the peak line-of-sight-integrated soot volume fraction ($\int f_v dr$). It is noted again that although there is quantitative difference between experiment and simulation, the numerical model successfully captured the measured qualitative trends of all three quantities. Both experiment and simulation show that with the increase in pressure, all three quantities increase. However, the rates of increase of the three quantities differ. This is qualitatively in agreement with the observation of McCrain and Roberts [2]. The measured three quantities approximately depend on pressure to the n th power, with $n \cong 2.03$, 1.31 and 1.65 for the

peak soot volume fraction, the peak area-integrated soot volume fraction and the peak line-of-sight-integrated soot volume fraction, respectively. This is also consistent with the findings of other studies [1-6]. The measured values of n are slightly higher than the calculated. We note that quantitatively the pressure exponent of the peak line-of-sight-integrated soot volume fraction ($\cong 1.65$) is slightly different from that obtained by Flower and Bowman [1] ($\cong 1.2$) for ethylene/air diffusion flame at pressures from 1 to 10 atm. It is not clear what causes the difference, but the experimental conditions (burner, fuel flow rates, etc.) in the two studies are different. Flower and Bowman [1] did not provide the pressure exponents for the peak soot volume fraction and the peak area-integrated soot volume fraction.

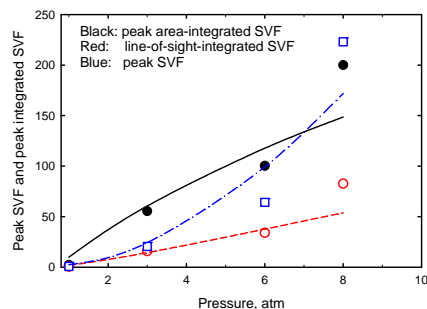


Fig. 2 Measured (symbols) and calculated (lines) peak SVF (ppm), peak area-integrated SVF ($ppm * mm^2$) and peak line-of-sight-integrated SVF ($ppm * mm$).

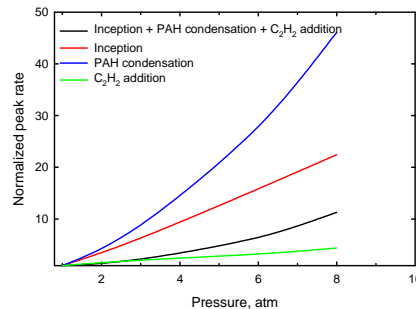


Fig. 3 Variations of normalized soot formation rates.

In order to understand the mechanisms of the effect of pressure on soot formation, details of simulation results are analyzed. In the numerical model employed in this paper, soot formation primarily consists of inception and surface growth. Surface growth includes PAH condensation and acetylene addition. Figure 3 shows the variations of normalized peak integrated total soot formation rate (inception + PAH condensation + C_2H_2 addition), inception rate, PAH condensation rate and acetylene addition rate. Each of these integrated rates was obtained by $\int 2\pi\omega_i r dr$, with ω_i being the rate. The normalized peak quantity is obtained by dividing the maximum integrated rate along the flame height at a pressure by the corresponding value at 1 atm. We observe from Fig. 3 that with the increase in pressure, all of these rates increase. However, the increase rates differ, with the increase rate of PAH condensation being the fastest and that of the acetylene addition being the slowest. The increase rate of inception is between those of PAH condensation and acetylene addition. The difference among the increase rates of inception, PAH condensation and acetylene addition suggests that the increase in pressure may result in the change in the relative contributions of the three soot formation sub-processes. This is confirmed by Fig. 4 that displays the distributions of integrated soot inception, PAH condensation and acetylene addition rates along flame height. It is revealed that at 1 atm, acetylene addition dominates soot formation. However, with the increase in pressure, PAH condensation rate quickly increases and finally significantly exceeds acetylene addition rate at pressures of 6 and 8 atm. Inception rate is lower than PAH condensation and acetylene addition rates at all pressures, but its relative contribution increases at higher pressures. Therefore, the increase in pressure causes not only the increase in total soot formation rate, but also the variation in the mechanisms of soot formation. This has never been reported before, since previous numerical studies [7-9] for soot formation at higher pressures did not include PAH in the reaction schemes.

The variation in the relative contributions of inception, PAH condensation and acetylene addition results from the different changing rates of temperature and concentrations of some key species related to soot formation. Although not shown due to space limit, simulation results show that temperature actually slightly decreases in soot formation region with the increase in pressure, primarily due to the

increase in radiation heat loss from soot. Therefore, temperature can be excluded from the factors that result in the increase in soot formation rate and the variation in the relative contributions of the three sub-processes. Figure 5 displays the variations in the normalized peak mole concentrations of three key species in soot formation, acetylene, pyrene and H radical. Similarly, the normalized concentration was obtained by dividing the mole concentration at a pressure by the corresponding value at 1 atm. It is observed that although the mole concentrations of acetylene and pyrene quickly increase, the mole concentration of radical H remains almost constant, when pressure increases. The variations in the concentrations of the three species can explain the observation in Figs. 3 and 4.

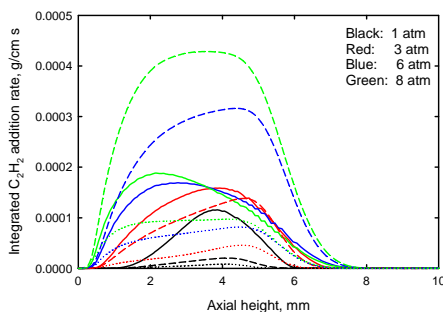


Fig. 4 Integrated inception (dotted), PAH condensation (dashed) and acetylene addition rates (solid).

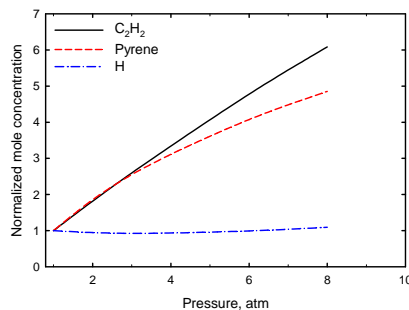


Fig. 5 Variations of normalized mole concentrations of C_2H_2 , pyrene and H.

In the soot model employed, particle inception is assumed to be due to the coalescence of two pyrene molecules. As a result, the increase in the mole concentration of pyrene results in the increase in the inception rate, when pressure increases. PAH condensation is assumed to be due to the collision between pyrene molecules and particle surface, and thus the PAH condensation rate depends on both the concentration of pyrene and particle surface area that is closely related to particle number density and inception rate. Therefore, the dependence of PAH condensation rate on pressure is stronger than that of inception rate. Acetylene addition is calculated by the model of HACA (hydrogen-abstraction-carbon-addition) [16] in which the rate of acetylene addition depends on temperature and concentrations of acetylene and radical H. Although the mole concentration of acetylene quickly increases with increasing pressure, the almost unchanged concentration of radical H and slightly decreased temperature cause the rate of acetylene addition to increase more slowly than those of inception and PAH condensation.

5. Concluding Remarks

Soot formation in laminar ethylene/air diffusion flames at pressures from 1 to 8 atm was investigated by experiment and numerical simulation using complex chemistry and a relatively detailed soot model. The numerical simulation successfully captured the qualitatively trend of pressure effect on soot formation. Both experiment and simulation show that soot volume fraction increases and the radial position of the maximum soot volume fraction moves toward the centerline, as pressure increases. The peak soot volume fraction and peak integrated soot volume fractions are approximately proportional to p^n . Further analysis of details of numerical results suggests that the increase in pressure also results in the variation in the mechanism of soot formation. At atmosphere pressure, soot formation is dominated by acetylene addition, followed by PAH condensation and inception. However, the contribution of PAH condensation quickly increase with pressure and finally significantly exceeds the contribution of acetylene addition at pressures of 6 and 8 atm.

Acknowledgement

Funding for this work was provided by Natural Resources Canada through the Program of Energy Research and Development, AFTER Project C23.006. ZG acknowledges the financial support of the Jiangsu Government Scholarship for Overseas Studies (JS-2006-024) and the National Natural Science Foundation of China (No.50778090).

References

- [1]. Flower W., Bowman CT. (1986). Soot production in axisymmetric laminar diffusion flames at pressures from one to ten atmospheres. *Proc. Comb. Inst.* 21: 1115.
- [2]. McCrain LL, Roberts WL. (2005). Measurements of the soot volume field in laminar diffusion flames at elevated pressures. *Combust. Flame.* 140: 60.
- [3]. Thomson K, Gülder ÖL, Weckman EJ, Fraser RA, Smallwood GJ, Snelling DR. (2005). Soot concentration and temperature measurements in co-annular, nonpremixed CH₄/air laminar flames at pressures up to 4 MPa. *Proc. Combust. Flame.* 140: 222.
- [4]. Joo HI, Gülder ÖL. (2009). Soot formation and temperature field structure in co-flow laminar methane-air diffusion flames at pressures from 10 to 60 atm. *Proc. Comb. Inst.* 32: 769.
- [5]. Bento DS, Thomson KA, Gülder ÖL. (2006). Soot formation and temperature field structure in laminar propane-air diffusion flames at elevated pressures. *Combust. Flame.* 145: 765.
- [6]. Mandatori PM, Gülder ÖL. (2010). Soot formation in laminar ethane diffusion flames at pressures from 0.2 to 3.3 MPa. *Proc. Comb. Inst.* 33: (in press).
- [7]. Zhang Z, Ezekoye OA. (1998). Soot production rate calculations at elevated pressure in a methane-air jet diffusion flame. *Combust. Sci. Tech.* 137: 323.
- [8]. Liu F, Thomson KA, Guo H, Smallwood GJ. (2006). Numerical and experimental study of an axisymmetric coflow laminar methane-air diffusion flame at pressures between 5 and 40 atmospheres. *Combust. Flame.* 164: 456.
- [9]. Charest MRJ, Joo HI, Gülder ÖL, Growth CPT. (2010). Experimental and numerical study of soot formation in laminar ethylene diffusion flames at elevated pressures from 10 to 35 atm. *Proc. Comb. Inst.* 33: (in press).
- [10]. Guo H., Liu F., Smallwood GJ, Gülder ÖL. (2006). A Numerical Study on the Influence of Hydrogen Addition on Soot Formation in a Laminar Ethylene-Air Diffusion Flame. *Combust. Flame.* 145: 324.
- [11]. Guo H., Thomson KA, Smallwood GJ. (2009). On the Effect of Carbon Monoxide Addition on Soot Formation in a Laminar Ethylene/Air Coflow Diffusion Flame. *Combust. Flame.* 156: 1135.
- [12]. Thomson KA, Johnson MJ, Snelling DR, Smallwood GJ. (2008). Diffuse-light two-dimensional line-of-sight attenuation for soot concentration measurements. *Applied Optics* 47: 694.
- [13]. Patankar SV. (1980). *Numerical heat transfer and fluid flow.* Hemisphere, New York.
- [14]. Liu F, Guo H, Smallwood GJ, Gülder Ö.L. (2004). Effects of radiation model on the modeling of a laminar coflow methane/air diffusion flame. *Combust. Flame.* 138: 136.
- [15]. Frenklach M, Wang H. (1994). Detailed Mechanism and Modeling of Soot Particle Formation. *Soot Formation in Combustion: Mechanisms and Models* (Bockhorn H, eEds). 59: 162.
- [16]. Appel J, Bockhorn H, Frenklach M. (2000). Kinetic modelling of soot formation with detailed chemistry and physics: Laminar premixed flames of C₂ hydrocarbons. *Combust. Flame.* 121: 122.